buildings

MDPI

Article

Calculation Method of Axial Compressive Capacity of 7075-T6 Aluminum Alloy Rectangular Tubes Based on Continuous Strength Method

Zhiguan Huang [1], Hailin Li [2], Cheng Zhang [3] and Junli Liu [3,*]

[1] Guangxi Guitong Engineering Management Group Co., Ltd., Nanning 532704, China; huangzg34@outlook.com
[2] Guangxi Airport Management Group Nanning Wuwei International Airport Co., Ltd., Nanning 530227, China; lhailin755@gmail.com
[3] Guangxi Key Laboratory of Green Building Materials and Construction Industrialization, Guilin University of Technology, Gui'lin 541004, China; zc1lzy@outlook.com
* Correspondence: 2003071@glut.edu.cn

Abstract

This study systematically investigates the axial compression capacity calculation method for 7075-T6 aluminum alloy rectangular hollow section (RHS) members based on the Continuous Strength Method (CSM). Axial compression tests were conducted on nine RHS specimens using a YAW-500 electro-hydraulic servo testing machine, and nonlinear finite element models considering material plasticity and geometric imperfections were established using ABAQUS/CAE. The numerical results showed good agreement with experimental data, verifying the model's reliability. Parametric analysis was then performed on RHS members, leading to the development of a CSM-based capacity calculation method and a modified curve for predicting the stability reduction factors of square hollow section members. The approach combining this modified curve with Chinese codes is termed the Modified Chinese Code Method. The axial capacities calculated by the CSM-based method, Modified Chinese Code Method, EN 1999-1-1, and AASTM were compared for accuracy evaluation. The conclusions indicate that the proposed modified curve provides more accurate predictions of stability coefficients for square tubes, and the CSM-based method yields more precise capacity predictions than existing international design codes, though it may overestimate the capacity for Class 4 cross-section members and thus requires further refinement.

Keywords: aluminum alloy structure; axial compression test; continuous strength method

Academic Editors: Adil Tamimi, Anderson Chu, Haodao Li, Yucun Gu and Baoquan Cheng

Received: 8 April 2025
Revised: 7 June 2025
Accepted: 15 June 2025
Published: 8 July 2025

Citation: Huang, Z.; Li, H.; Zhang, C.; Liu, J. Calculation Method of Axial Compressive Capacity of 7075-T6 Aluminum Alloy Rectangular Tubes Based on Continuous Strength Method. *Buildings* **2025**, *15*, 2387. https://doi.org/10.3390/buildings15142387

1. Introduction

Aluminum alloys, with their lightweight, high strength, corrosion resistance, and aesthetic appearance, are widely used in engineering applications such as pedestrian bridges, grid structures, and other civil engineering projects [1]. At the same time, aluminum alloys have a very high recycling rate, typically ranging from 95% to 98%, and recycled aluminum alloys can restore their original properties, offering significant environmental benefits [2]. However, the modulus of elasticity of aluminum alloys is relatively low, approximately one-third that of steel, and coupled with the high strength of aluminum alloys, this leads to typically slender section designs. Therefore, local stability remains a prominent issue [3]. If the design approach used for steel structures is adopted, where aluminum alloy components are required to avoid local buckling before overall failure, i.e., not relying on the

post-buckling strength of the material, the width-to-thickness ratio of compressed plate components must be smaller, which results in very uneconomical section designs [4,5]. To address this, both the "Code for Design of Aluminum Structures" (GB 50429-2007 [4]) and the European Standard EN 1999-1-1:2007+A1 [6] employ the effective section method to take advantage of the post-buckling strength of aluminum alloys. The effective section method treats the individual plate components of a member as independent entities, calculating the effective thickness of each plate and then determining the effective section. However, the interaction between the plates, such as between flange plates and web plates, which enhances the section's load-bearing capacity, is not considered in the effective section method. This interaction is known as the plate group effect [7,8].

In addition, the stress-strain curve of aluminum alloys does not exhibit a distinct yield plateau but instead follows a continuous and smooth curve [9]. Both the "Code for Design of Aluminum Structures" (GB 50429-2007 [4]) and the European Standard EN 1999-1-1:2007+A1 [6] adopt an ideal elastic-plastic model as the material constitutive model, neglecting the strain-hardening behavior of aluminum alloys. Therefore, designs based on these standards typically make more conservative predictions regarding the load-bearing capacity of aluminum alloy components.

To address the aforementioned issues, the Continuous Strength Method (CSM) can be used to calculate the load-bearing capacity of aluminum alloy components. The CSM was first proposed by Leroy Gardner and others [10]. It moves away from the traditional design approach based on section classification and instead determines the compressive and bending strength of a member based on its deformation capacity. The method fully considers the strain-hardening characteristics of the material and the plate group effect of the member [10]. The CSM is particularly suitable for materials with nonlinear constitutive relationships, such as high-strength steel, stainless steel, and aluminum alloys [11].

Currently, research on the Continuous Strength Method, both Chinese and internationally primarily focuses on predicting the section strength of aluminum alloy components. Su et al. conducted experimental and finite element simulations on aluminum alloy short-columns and beams with different section types and found that the CSM is able to more accurately predict the section strength of aluminum alloy components compared with the calculation methods in current national codes, and it fully utilizes the strain-hardening capacity of the aluminum alloy material [12–16]. Marina et al. studied the biaxial bending of aluminum alloy rectangular tubes [17], while Craig et al. investigated the compression and bending behavior of aluminum alloy circular tubes, both of which validated the accuracy of the CSM in predicting the section strength of aluminum alloy components [18]. Xiang-Rong Chen et al. combined the calculation method in the Chinese Aluminum Structure Design Code (GB 50429-2007) [4] with the Continuous Strength Method and proposed a calculation method for the axial compressive load-bearing capacity of aluminum alloy rectangular tubes based on the CSM. They found that the stability load-bearing capacity predictions in the Chinese aluminum code are generally conservative for components with a section flexibility factor in the range of 0.228 to 0.906, especially for components with large slenderness ratios, where the stability load-bearing capacity predictions are notably more conservative [19]. Zhai Ximei, Zhao Yuanzheng, and others conducted experiments on 6082-T6 aluminum alloy members and compared the experimental results with the current American Aluminum Design Manual [20,21], European Aluminum Structure Design Code [6], Chinese Aluminum Structure Design Code (GB 50429-2007) [4], as well as the computational results from the Direct Strength Method and Continuous Strength Method. They analyzed and evaluated the computational accuracy of each method [22–26]. Chen et al. [27] performed tests on 11 short column specimens made of 7A04-T6 and 6061-T6 aluminum alloys. Through experimental validation, they applied a finite element model to a

series of comprehensive parametric studies and proposed a new CSM (Continuous Strength Method) relationship to determine the compressive sectional resistance of high-strength non-slender CHS (Circular Hollow Section) aluminum alloy members.

Currently, the commonly used 6000-series aluminum alloy materials in engineering structures have a yield strength of around 200 MPa, while the yield strength of 7000-series aluminum alloys can reach up to 500 MPa. To explore the application of 7000-series aluminum alloys in engineering structures, this study will focus on 7075-T6 rectangular tubes as the research object. Based on the axial compressive tests of nine 7075-T6 aluminum alloy rectangular tube specimens, the axial compressive load-bearing capacity will be calculated using the Continuous Strength Method (CSM). The results obtained from the CSM, the design code methods, and the experimental results will be compared.

2. The Axial Compression Test

To study the axial compression performance of 7075-T6 aluminum alloy rectangular tubes and provide a basis for validating finite element numerical analysis and the development of load-bearing capacity calculation methods based on the Continuous Strength Method, nine 7075-T6 aluminum alloy rectangular tube specimens were designed with the cross-section width-to-thickness ratio and member slenderness ratio as variables. Axial compression tests were conducted.

2.1. Tensile Test of Materials

According to "Metallic Materials—Tensile Testing—Part 1: Method of Test at Room Temperature" (GB/T 228.1-2021 or ISO 6892-1) [28], tensile specimens were cut along the longitudinal direction of the aluminum alloy square tubes for material tensile testing. For each cross-sectional dimension of the tubes, three tensile specimens were extracted. The dimensions of the specimens varied depending on the tube's cross-sectional specifications, as illustrated in Figure 1. The tensile tests were conducted using a hydraulic universal testing machine, and use high-precision extensometer with a gauge length of 50 mm was used to measure its strain, as shown in Figure 2.

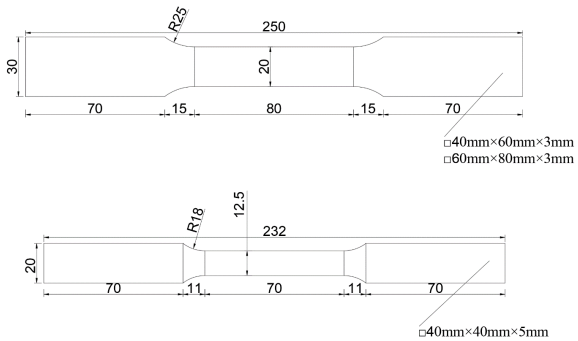

Figure 1. Tensile specimen dimension (Unit: mm).

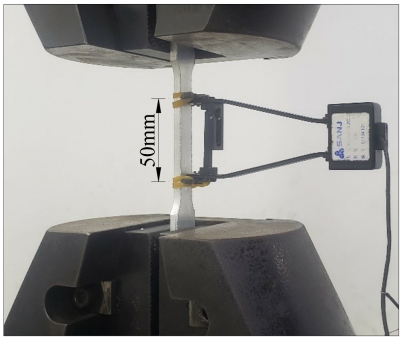

Figure 2. Tensile testing equipment.

Regarding the constitutive relationship of aluminum alloy materials, the most widely used model is the Ramberg-Osgood model [29]. Proposed by Ramberg and Osgood in 1939, this model employs three material parameters to describe the stress-strain behavior of aluminum alloys. The constitutive equation of the Ramberg-Osgood model is expressed as follows:

$$\varepsilon = \frac{\sigma}{E} + 0.002\left(\frac{f_{0.2}}{E}\right)^{n} \tag{1}$$

in the equation, E represents the elastic modulus at the origin; $f_{0.2}$ denotes the nominal yield strength at 0.2% plastic strain; n is the strain-hardening exponent, reflecting the material's strain-hardening capability. Among these parameters, E and $f_{0.2}$ can be directly measured through tensile testing, where n cannot be obtained directly from material tensile tests. In practical calculations, the approximate formula proposed by SteinHardt (1971) [30] is commonly employed , as expressed below:

$$n = 0.1 f_{0.2} \tag{2}$$

Based on the material tensile test results and SteinHardt's proposed formula, the constitutive parameters of 7075-T6 aluminum alloy were determined as follows: Elastic modulus at the origin (E): 76.04 GPa; Nominal yield strength at 0.2% plastic strain ($f_{0.2}$): 418.03 MPa; Ultimate tensile strength (f_u): 498.9 MPa; Strain-hardening exponent (n): 41.8. The constitutive relationship curve of the 7075-T6 aluminum alloy is illustrated in Figure 3. The tensile results of the specimens are listed in Table 1.

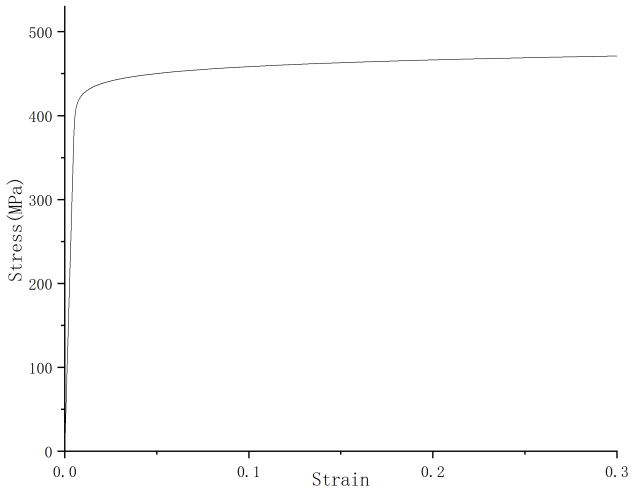

Figure 3. Constitutive relationship curve of 7075-T6 aluminum alloy.

Table 1. Material tensile test results.

Tensile Specimen	*E*/MPa	$f_{0.1}$/MPa	$f_{0.2}$/MPa	f_u
T-1	74,360	309.43	322.06	423.77
T-2	76,460	364.63	375.55	462.99
T-3	77,000	472.73	483.79	575.64
T-4	78,840	359.69	372.16	460.48
T-5	79,540	549.03	557.27	607.44
T-6	74,710	432.96	443.94	509.84
T-7	73,210	463.59	473.82	541.41
T-8	76,310	360.7	371.35	457.47
T-9	73,910	350.92	362.33	451.02

2.2. Specimen Design

In this study, nine 7075-T6 aluminum alloy rectangular tube specimens were designed with the cross-section width-to-thickness ratio and member slenderness ratio as variables. The rectangular tube specimens were produced by Shanghai Jiehao Metal Products Co., Ltd., Shanghai, China. The specimens had three cross-sectional dimensions: 40 mm × 40 mm × 5 mm, 40 mm × 60 mm × 3 mm, and 60 mm × 80 mm × 3 mm, with the width-to-thickness ratio ranging from 6 to 24.67. Three slenderness ratios were set for the specimens: 30, 45, and 60 [31]. The cross-sectional dimensions of the rectangular tube specimens are shown in the figure below. Detailed information about the rectangular tube specimens is summarized in Figure 4.

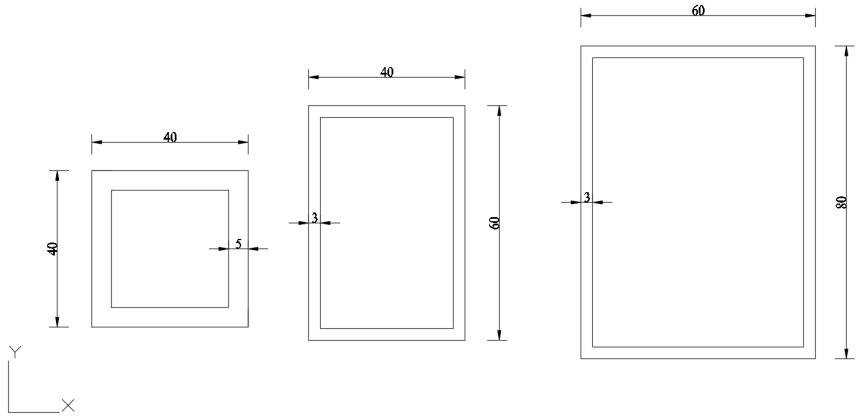

Figure 4. Schematic diagram of cross-sectional dimensions (unit: mm).

In Table 2, taking the specimen number "60-40-3-45" as an example to explain the numbering convention, "60" indicates that the height of the specimen's cross-section is 60 mm, "40" indicates that the width of the specimen's cross-section is 40 mm, "3" indicates that the thickness of the cross-section is 3 mm, and "45" indicates the preset slenderness ratio of the specimen is 45.

Table 2. Summary of specific information on rectangular tube specimens.

Specimen Number	Cross-Sectional Dimensions /mm	Preset Slenderness Ratio	Measured Cross-Sectional Height /mm	Measured Cross-Sectional Width /mm	Measured Cross-Sectional Thickness /mm	Actual Height /mm	Actual Slenderness Ratio
40-40-5-30	40 × 40 × 5	30	39.94	40.01	4.99	493	34.2
40-40-5-45	40 × 40 × 5	45	40.01	39.96	5	710	49.24
40-40-5-60	40 × 40 × 5	60	39.98	39.98	4.99	926	64.18
60-40-3-30	60 × 40 × 3	30	60.01	40.03	2.99	562	35.24
60-40-3-45	60 × 40 × 3	45	60.01	40.01	3	729	45.75
60-40-3-60	60 × 40 × 3	60	60.02	40.1	2.99	981	61.42
80-60-3-30	80 × 60 × 3	30	79.94	59.95	2.96	785	32.51
80-60-3-45	80 × 60 × 3	45	80.09	59.88	2.97	1146	47.51
80-60-3-60	80 × 60 × 3	60	79.94	59.92	2.97	1509	62.53

2.3. Axial Compression Test Plan

The axial compression tests on 7075-T6 aluminum alloy rectangular tubes were conducted using a YAW-500 electro-hydraulic servo long-column testing machine from Jinan Shijin Group Co., LTD., Jinan, China, as shown in Figure 5.

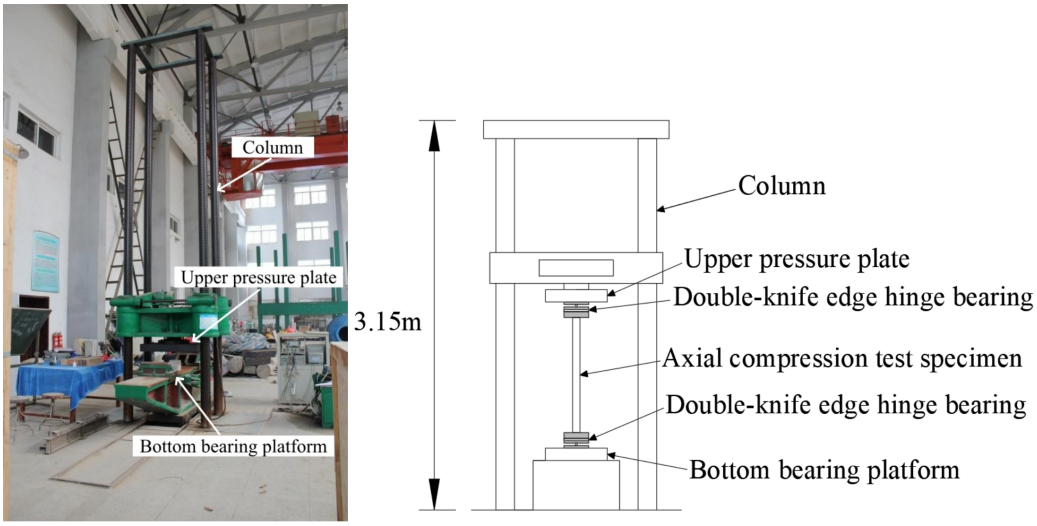

Figure 5. YAW-500 electro-hydraulic servo long column testing machine.

The top of the testing machine is equipped with a reaction frame, which includes a spherical hinge to simulate a pinned connection at the upper end. When installing the specimen, the lower end of the specimen is placed in a bidirectional hinge support to achieve a pinned-pinned boundary condition. The bidirectional hinge support consists of three steel plates with arc grooves and two cylindrical steel blocks. A 3D rendering of the bidirectional hinge support is shown in Figure 6. During installation, the box-shaped clamping block is first fixed to the upper part of the support using bolts, creating a reserved slot. The lower end of the specimen is then installed into the box-shaped slot. The installation effect of the specimen is shown in Figure 7. To ensure that the specimen is subjected to axial compression during the test, the specimen should be aligned so that the geometric center of its cross-section coincides with the geometric center of the supports at both ends while maintaining the verticality of the specimen.

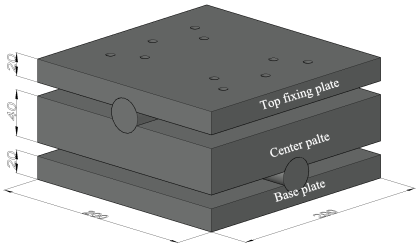

Figure 6. Schematic diagram of the three-dimensional effect of the support.

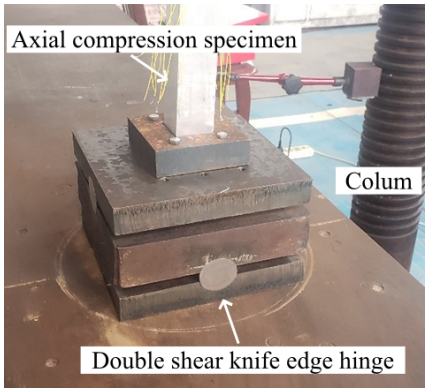

Figure 7. Actual installation effect of specimen.

During the test loading process, the axial displacement of the specimen, the strain at specific points near the mid-span, and the applied load values were recorded. The load was applied from the bottom to the top. To measure the axial displacement at the loading end, four dial gauges were arranged around the loading end to capture the displacement. The average value of the displacements measured by the four dial gauges at each load level was taken as the representative displacement value for that load level. The actual arrangement of the dial gauges is shown in Figure 8.

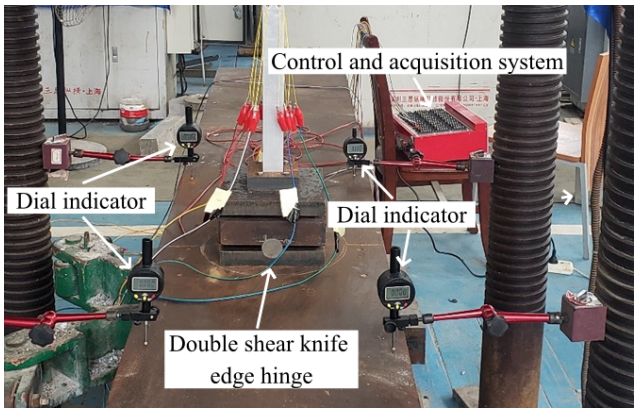

Figure 8. Actual arrangement of the dial gauge.

To further investigate the failure modes of the specimens, eight strain gauges were arranged at the mid-span, where failure was most likely to occur. The centers of the strain gauges were positioned 5 mm from the nearest edge of the plate. The strain gauges were labeled from 1 to 9, and their data were collected using an XL2118A static resistance strain gauge. The arrangement of the strain gauges is shown in Figure 9. As for the load values, they were collected through the electronic data acquisition system integrated into the testing machine.

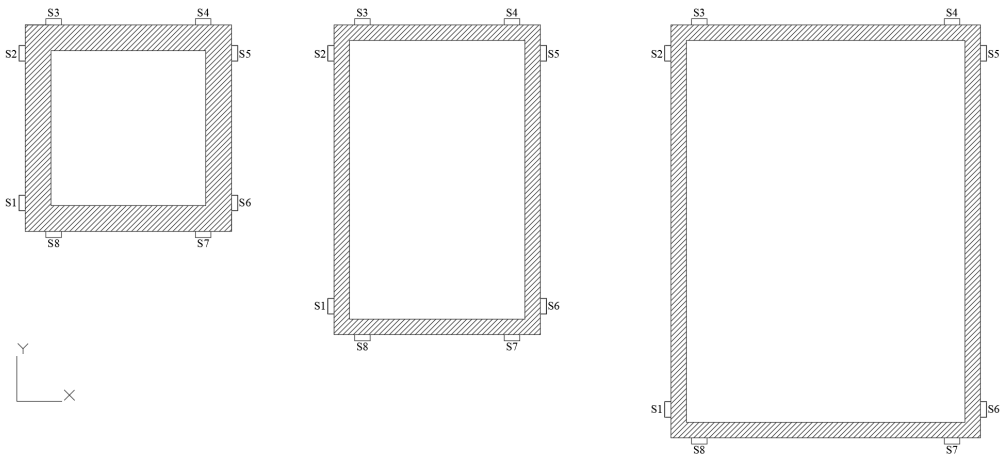

Figure 9. Schematic diagram of strain gauge arrangement.

Axial compression tests were conducted on all specimens. The stress was downward along the axis, and the subjected load had a monotonic increment: (1) At the initial stage of the test, each load increment was set at 5 kN, with a holding period of 2–3 min to facilitate data acquisition; (2) When the displacement increased without a significant change in the load data, the loading mode was switched to displacement control, and slow loading was applied until the specimen exhibited pronounced deformation and the load data demonstrated a significant decline, at which point the loading was terminated. The

experimental results for the ultimate load-bearing capacity are presented in Table 3, in the table, "C" is "Complete buckling", "L" is "Local buckling".

Table 3. Ultimate Load-Bearing Capacity Test Results.

Specimen Number	40-40-5-30	40-40-5-45	40-40-5-60	60-40-3-30	60-40-3-45	60-40-3-60	80-60-3-30	80-60-3-45	80-60-3-60
Test Results σ_t/MPa	388.1	319.6	192.3	442.6	262.2	192.9	297.9	230.1	172.5
Form of destruction	C	C	C	L	C	C	C	C	C

2.4. Finite Element Model Validation

In this study, the finite element analysis software ABAQUS was employed to establish a finite element (FE) model of the experimental specimens. The material properties of the model, with parameters determined from material tensile tests, were assigned based on the numerical values provided in Sections 2.1 and 2.2. A buckling analysis was performed on the finite element (FE) model of the specimens. After obtaining the buckling modes at various orders, the appropriate buckling mode was selected and introduced as an initial imperfection into the FE model based on the failure modes observed in the experiments.

The load-bearing capacity results obtained from finite element (FE) numerical analysis are summarized in Table 4. The mean absolute error between the experimentally measured and FE-predicted load-bearing capacities was 6.91%. Based on the results in Table 4, it can be concluded that the established FE model accurately calculates the axial compressive capacity of 7075-T6 square tubes and is validated for further parametric analysis.

Table 4. Comparison of ultimate load-bearing capacity.

Specimen Number	Test Results σ_t/MPa	Finite Element Results σ_{FEA}/MPa	Difference/%
40-40-5-30	388.1	412.1	6.18
40-40-5-45	319.6	315.4	−1.3
40-40-5-60	192.3	203.1	5.65
60-40-3-30	442.6	407.4	−7.93
60-40-3-45	262.2	283.3	8.05
60-40-3-60	192.9	176.1	−8.73
80-60-3-30	297.9	329.1	10.48
80-60-3-45	230.1	246.1	6.97
80-60-3-60	172.5	186.3	6.18

The comparison between the experimental failure modes of all specimens and the finite element (FE)-predicted failure modes is illustrated in Figure 10. We marked the specimens in the picture, and the specific dimensions of the specimens are shown in Table 2. Figure 11 compares the experimental load-axial displacement curve of the typical specimen 80-60-3-30 with the FE-predicted load-axial displacement curve, demonstrating that the two curves exhibit consistent trends in their overall behavior.

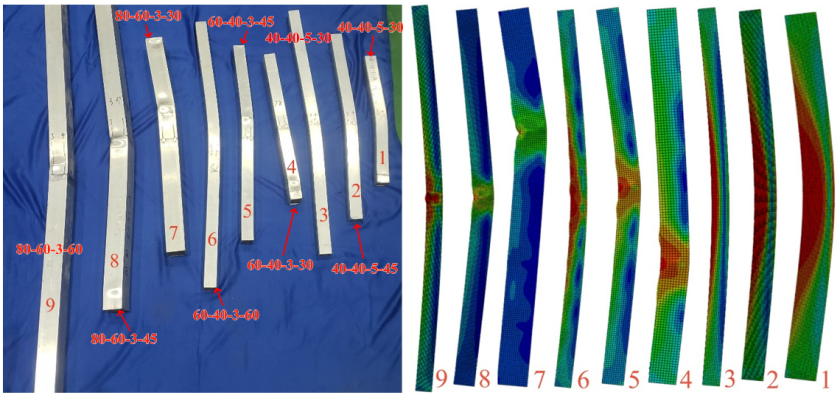

Figure 10. Comparison of failure modes between all specimen tests and finite element analysis.

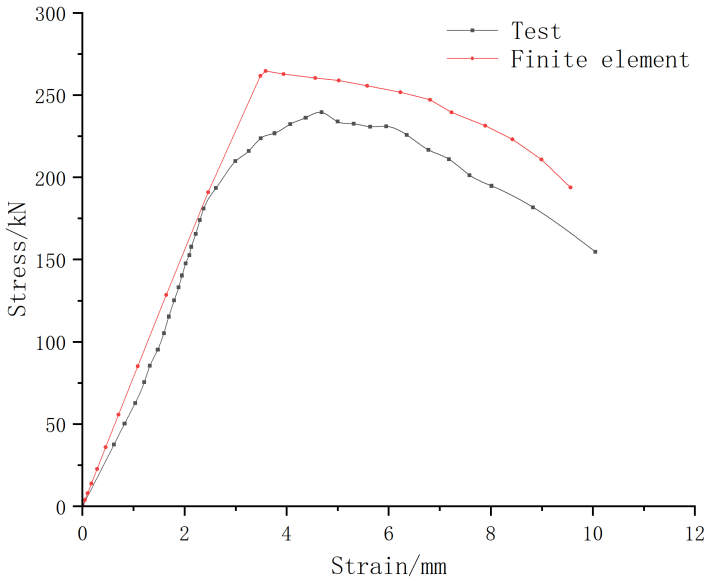

Figure 11. Comparison of load axial-displacement curve.

3. Current Standard Calculation Method

3.1. Chinese Standards

According to Chinese standards [4], the calculation formula for the axial compressive capacity of aluminum alloy components is as follows:

$$N = f_{0.2}\eta_e\eta_{haz}\varphi A \tag{3}$$

where N is the axial compressive load-bearing capacity of the aluminum alloy component, $f_{0.2}$ denotes the nominal yield strength of the aluminum alloy material, η_e is the effective section coefficient considering the effect of local buckling, which is calculated using the effective thickness method, η_{haz} is the welding defect influence factor, φ represents the stability factor, and A is the gross cross-sectional area of the member.

For the calculation of the stability factor φ, Chinese codes assume that the component has an initial overall geometric imperfection with a half-wave sinusoidal shape. Based on the edge yield criterion, the stability load-bearing capacity is calculated using the following formula:

$$\frac{P}{A}\left[1 + \frac{Ae_0}{W(1 - \frac{P}{P_E})}\right] = f_{0.2} \tag{4}$$

where e_0 represents the initial overall geometric defect amplitude, W denotes the gross section modulus of the member, P_E indicates the Euler critical load, and P is the stable load-bearing capacity. Introducing the equivalent defect coefficient $\varepsilon_0 = Ae_0/W$, Equation (4) can be rewritten as follows:

$$\frac{P}{A}\left[1 + \frac{\varepsilon_0}{(1 - \frac{P}{P_E})}\right] = f_{0.2} \tag{5}$$

for the stability load-bearing capacity P in Equation (5), dividing by $Af_{0.2}$ and letting $\varphi = P/Af_{0.2}$ yields the expression for the stability factor φ, which is the Perry-Roberson formula.

$$\varphi = \frac{1}{\bar{\lambda}^2}\left[(1 + \varepsilon_0 + \bar{\lambda}^2) - \sqrt{(1 + \varepsilon_0 + \bar{\lambda}^2)^2 - 4\bar{\lambda}^2}\right] \tag{6}$$

where $\bar{\lambda}$ represents the relative slenderness ratio of the component, calculated according to the following formula:

$$\bar{\lambda} = \sqrt{\frac{f_{0.2}}{\sigma_E}} \tag{7}$$

The equivalent imperfection factor ε_0 in Equation (5) is calculated as follows:

$$\varepsilon_0 = \frac{Ae_0}{W} = \alpha(\bar{\lambda} - \bar{\lambda}_0) \tag{8}$$

for 7075-T6 aluminum alloy materials, the analytical results yield parameters α is taken as 0.08 and $\bar{\lambda}_0$ is taken as 0.17 [4].

3.2. Eurocode 9

According to relevant specifications in EN 1999 (Eurocode 9: Design of aluminum structures) [6], the design buckling resistance of a compression member $N_{b,Rd}$ should be taken as:

$$N_{b,Rd} = \kappa\chi A_{\text{eff}} f_0/\gamma_{M1} \tag{9}$$

In this equation, χ is the reduction factor for the relevant buckling mode that can be calculated in Equation (10); κ is a factor to allow for the weakening effects of welding; A_{eff} is the effective area allowing for local buckling for class 4 cross-sections, and $A_{\text{eff}} = A$ for class 1, 2, and 3 cross-sections.

For axial compression in members, the value of χ for the appropriate value of $\bar{\lambda}$ should be determined from the relevant buckling curve according to

$$\chi = \frac{1}{\phi + \sqrt{\phi^2 - \bar{\lambda}^2}}, \chi \leq 1.0 \tag{10}$$

where $\phi = 0.5(1 + \alpha(\bar{\lambda} - \bar{\lambda}_0) + \bar{\lambda}^2)$, $\bar{\lambda} = \sqrt{\frac{A_{\text{eff}} f_{0.2}}{N_{cr}}}$, α is an imperfection factor, $\bar{\lambda}_0$ is the limit of the horizontal plateau, N_{cr} is the elastic critical force for the relevant buckling mode based on the gross cross-sectional properties.

3.3. Aluminum Association AA ADM-2020

In the Aluminum Association Design Manual (AA ADM-2020) [21], the nominal member buckling strength P_{nc} is

$$P_{nc} = F_c A_g \tag{11}$$

where A_g is gross cross-sectional area; F_c is stress corresponding to flexural strength and can be calculated by Equation (12):

$$F_c = \begin{cases} F_{cy} & ,\lambda \le \frac{B_c - F_{cy}}{D_c} = \lambda_1 \\ (B_c - D_c\lambda)(0.85 + 0.15(\frac{C_c - \lambda}{C_c - \lambda_1})) & ,\frac{B_c - F_{cy}}{D_c} < \lambda < C_c \\ \frac{0.85\pi^2 E}{\lambda^2} & ,\lambda \ge C_c \end{cases} \quad (12)$$

In this equation, B_c is the buckling constant intercept for member buckling; C_c is the buckling constant intersection for member buckling; D_c is the buckling constant slope for member buckling; F_{cy} is the compressive yield strength; E is the modulus of elasticity; λ is the slenderness; and λ_1 is the slenderness at the intersection of the equations for yielding and inelastic buckling.

4. Calculation Method Based on the Continuous Strength Method

The Continuous Strength Method (CSM) is a design approach that takes into account the material strain-hardening effects and is based on deformation. This method has two main characteristics: (1) fundamental curve, which describes the strain levels that a section can withstand at different local slenderness ratios, demonstrating the continuous relationship between the section's deformation capacity and slenderness ratio; (2) strain-hardening material model. Su et al. [13] proposed a fundamental curve and a bilinear constitutive model suitable for aluminum alloy rectangular tubes. This study will adopt the fundamental curve and bilinear constitutive model from reference [13] for further research.

4.1. Base Curve

In the Continuous Strength Method, the section limit strain ε_{CSM} is used to evaluate the ultimate deformation capacity of the section, and the expression is as follows [13,14]:

$$\frac{\varepsilon_{CSM}}{\varepsilon_y} = \begin{cases} 0.25/\bar{\lambda}_p^{3.6}, \varepsilon_{CSM}/\varepsilon_y \le min(15, A_1\varepsilon_u/\varepsilon_y) & ,\bar{\lambda}_p \le 0.68 \\ (1 - 0.222/\bar{\lambda}_p^{1.05})(1/\bar{\lambda}_p^{1.05}) & ,\bar{\lambda}_p > 0.68 \end{cases} \quad (13)$$

where ε_y is the strain at material yield, ε_u represents the strain at the maximum stress of the material, and $\bar{\lambda}_p$ denotes the slenderness ratio of the section. In the Continuous Strength Method (CSM), the slenderness ratio $\bar{\lambda}_p$ is defined as the square root of the ratio of the yield stress f_y to the section's elastic buckling stress σ_{cr}:

$$\bar{\lambda}_p = \sqrt{\frac{f_y}{\sigma_{cr}}} \quad (14)$$

In the formula, the elastic buckling stress of the section σ_{cr} can be calculated using the approximate formula proposed by Seif [32] or by employing the finite strip software CUFSM developed by Johns Hopkins University [33].

4.2. Bilinear Constitutive Model

After determining the ultimate strain ε_{CSM} at the section from the fundamental curve, it is substituted into the material's constitutive model to obtain the section's strength f_{CSM} under the Continuous Strength Method. Since the stress-strain relationship of aluminum alloy materials is nonlinear, making the calculations relatively complex, the constitutive model is simplified to a linear strain-hardening elastoplastic model with the following expression:

$$f_{CSM} = \begin{cases} E\varepsilon_{CSM} & ,\varepsilon < \varepsilon_y \\ f_{0.2} + E_{sh}(\varepsilon - \varepsilon_y) & ,\varepsilon_y \le \varepsilon \le A_2\varepsilon_u \end{cases} \tag{15}$$

where E is the elastic modulus of the aluminum alloy, and the coefficient A_2 is determined by the material's strain-hardening capacity, used to control the upper limit of the material's strain-hardening degree. For aluminum alloy materials, A_2 = 0.5. E_{sh} represents the the strain-hardening modulus of the material, reflecting strain-hardening ability of the material. For different materials, it can be calculated by the following formula:

$$E_{sh} = \frac{f_u - f_{0.2}}{A_2\varepsilon_u - \varepsilon_y} \tag{16}$$

where f_u is the ultimate strength of the material.

4.3. Stability Coefficient

According to the calculation theory of the Continuous Strength Method, since the section strength f_{CSM} of the aluminum alloy component already accounts for the effect of local buckling, it is necessary to determine the stability factor φ_{CSM} of the component from the perspective of the Continuous Strength Method when calculating the load-bearing capacity of the aluminum alloy rectangular tube component. For the calculation of φ_{CSM}, the Perry-Roberson formula is still used:

$$\varphi_{CSM} = \frac{1}{\bar{\lambda}_{CSM}^2}\left[(1 + \varepsilon_{CSM} + \bar{\lambda}_{CSM}^2) - \sqrt{(1 + \varepsilon_{CSM} + \bar{\lambda}_{CSM}^2)^2 - 4\bar{\lambda}_{CSM}^2}\right] \tag{17}$$

where $\bar{\lambda}_{CSM}$ is the relative slenderness ratio of the component according to the Continuous Strength Method, referred to as the CSM relative slenderness ratio; ε_{CSM} represents the equivalent imperfection factor of the component according to the CSM, referred to as the CSM equivalent imperfection factor.

By replacing f_{CSM} and $\bar{\lambda}_{CSM}$ with $f_{0.2}$ and $\bar{\lambda}$ in Equation (7), the CSM relative slenderness ratio is obtained as follows:

$$\bar{\lambda}_{CSM} = \sqrt{\frac{f_{CSM}}{\sigma_E}} \tag{18}$$

Let e_{CSM} represent the initial overall geometric imperfection amplitude of the component under the Continuous Strength Method, referred to as the CSM initial imperfection amplitude. By substituting ε_{CSM}, f_{CSM}, and e_{CSM} for ε_0, $f_{0.2}$, and e_0 in Equations (4) and (5), the following results are obtained:

$$\frac{P}{A}\left[1 + \frac{Ae_{CSM}}{W\left(1 - \frac{P}{P_E}\right)}\right] = f_{CSM} \tag{19}$$

$$\frac{P}{A}\left[1 + \frac{\varepsilon_{CSM}}{W\left(1 - \frac{P}{P_E}\right)}\right] = f_{CSM} \tag{20}$$

Assume that the CSM equivalent imperfection factor can be calculated in the form of Equation (8), but there is an undetermined parameter α_{CSM}. By replacing α_{CSM}, $\bar{\lambda}_{CSM}$, and e_{CSM} with α, $\bar{\lambda}$ and e_0 in Equation (8), the calculation formula for the CSM equivalent imperfection factor is obtained as follows:

$$\varepsilon_{CSM} = \frac{Ae_{CSM}}{W} = \alpha_{CSM}(\bar{\lambda}_{CSM} - \bar{\lambda}_0) \tag{21}$$

In the equation, $\bar{\lambda}_{CSM}$ can be calculated using Equation (18), while $\bar{\lambda}_0$ is a known parameter, which for aluminum alloys is taken as 0.17 [4]. To calculate the undetermined parameter α_{CSM}, Equations (8) and (21) are solved simultaneously, yielding the following formula:

$$\alpha_{CSM} = \alpha \frac{e_{CSM}}{e_0} \frac{\bar{\lambda} - \bar{\lambda}_0}{\bar{\lambda}_{CSM} - \bar{\lambda}_0} \tag{22}$$

let $\beta = e_{CSM}/e_0$, then Equation (22) is

$$\alpha_{CSM} = \alpha\beta \frac{\bar{\lambda} - \bar{\lambda}_0}{\bar{\lambda}_{CSM} - \bar{\lambda}_0} \tag{23}$$

In Equation (23), the parameter α is taken as 0.08. All parameters except for β are determined. Therefore, once the parameter β is determined, α_{CSM} can be calculated using Equation (23), then ε_{CSM} (the CSM equivalent imperfection factor) can be calculated using Equation (21), and finally, the stability factor φ_{CSM} under the Continuous Strength Method can be calculated using Equation (17).

4.4. Calculation of Parameter β

The parameter β is the ratio of the CSM initial imperfection amplitude e_{CSM} to the initial overall geometric imperfection amplitude e_0. This means that when $\beta > 1$, from the perspective of the Continuous Strength Method, the component is allowed to have an initial overall geometric imperfection amplitude larger than e_0; conversely, if $\beta \leq 1$, it indicates that the initial overall geometric imperfection amplitude of the component should be less than or equal to e_0. When $\beta > 1$, $e_{CSM} > e_0$, and by substituting e_{CSM} into Equation (16) to calculate f_{CSM}, it results in $f_{CSM} > f_{0.2}$. This indicates that, from the perspective of the CSM, the section stress of the component should be greater than $f_{0.2}$. On the other hand, if $\beta \leq 1$, the section stress should be less than or equal to $f_{0.2}$. Therefore, the parameter β can be referred to as the strength development index in the Continuous Strength Method. Since β is an indicator related to strength development capacity, its value, under the condition that the material's ultimate strength f_u is not exceeded, should be related to both the overall and local stability of the component. The overall and local stability of the component is, in turn, associated with the "thickness" of the component and its section. In the Continuous Strength Method, the overall "thickness" of the component and the "thickness" of the section can be measured by the CSM relative slenderness ratio $\bar{\lambda}_{CSM}$ and the section slenderness ratio $\bar{\lambda}_p$, respectively. Therefore, it is assumed that the parameter β is a function of $\bar{\lambda}_{CSM}$ and $\bar{\lambda}_p$, i.e.,

$$\beta = f(\bar{\lambda}_{CSM}, \bar{\lambda}_p) \tag{24}$$

To investigate the relationship between β and $\bar{\lambda}_{CSM}$, $\bar{\lambda}_p$, based on the validated finite element (FE) model in Section 2.4, a parametric expansion was conducted by developing 215 FE models for analysis. These models include 15 different section specifications and 15 different relative slenderness ratios, with the section types covering the four categories defined by the European standards [6]. Specific details can be found in Table 5. To verify the accuracy of the finite element models, 9 section types were selected for axial compression capacity tests, and the test results are presented in Table 4.

The ultimate load-bearing capacity results of the 215 finite element models were substituted into Equations (4) and (19), respectively, to calculate the corresponding values of e_o and e_{CSM} for each finite element model and, subsequently, the corresponding β for

each model. Using $\bar{\lambda}_{CSM}$ as the x-axis, $\bar{\lambda}_p$ as the y-axis, and β as the z-axis, the three-dimensional scatter plots of the strength development index β for the finite element models were plotted for the two cases: $\bar{\lambda}_p \leq 0.68$ and $\bar{\lambda}_p > 0.68$. These plots are shown in Figures 12 and 13.

Table 5. Specific Information of the Finite Element Model.

Section Category	Section Dimensions	Section Slimness Ratio $\bar{\lambda}_p$	Relative Slenderness Ratio of the Member $\bar{\lambda}$
Type 1	80 × 80 × 10	0.28	0.6, 0.8, 1.0, 1.2, 1.4, 1.6, 1.8, 2.0, 2.2, 2.4, 2.6, 2.8, 3.0, 3.2, 3.4
	70 × 70 × 8	0.31	
	60 × 60 × 6	0.36	
Type 2	60 × 40 × 5	0.39	
	50 × 40 × 4	0.42	
	60 × 60 × 5	0.43	
	50 × 50 × 4	0.45	
Type 3	80 × 60 × 5	0.54	
	50 × 40 × 3	0.57	
	50 × 50 × 3	0.61	
Type	80 × 40 × 4	0.65	
	80 × 60 × 4	0.68	
	100 × 100 × 5	0.74	
	76 × 44 × 3	0.84	
	80 × 60 × 3	0.92	
	120 × 60 × 4	0.99	

From Figures 12 and 13, it can be seen that in the three-dimensional space defined by the parameters $\bar{\lambda}_{CSM}$, $\bar{\lambda}_p$, and β, all the three-dimensional scatter points are distributed in a certain pattern. This indicates that there is a correlation between the parameter β and the parameters $\bar{\lambda}_{CSM}$ and $\bar{\lambda}_p$, which validates the reasonableness of the hypothesis in Equation (20). Additionally, from Figures 12 and 13, it can be observed that the distribution pattern of the scatter points is different in the two cases. Therefore, based on the different scatter point distributions, the nonlinear fitting function in the data analysis software Origin should be used to determine the quantitative relationship between β and $\bar{\lambda}_{CSM}$, $\bar{\lambda}_p$.

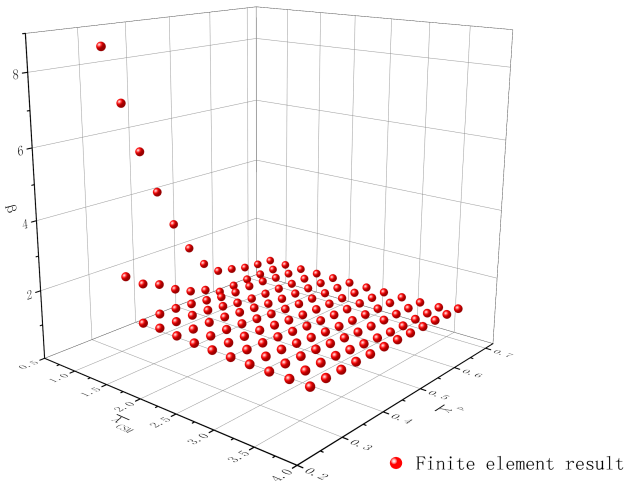

Figure 12. Scatter distribution of finite element results when $\bar{\lambda}_p \leq 0.68$.

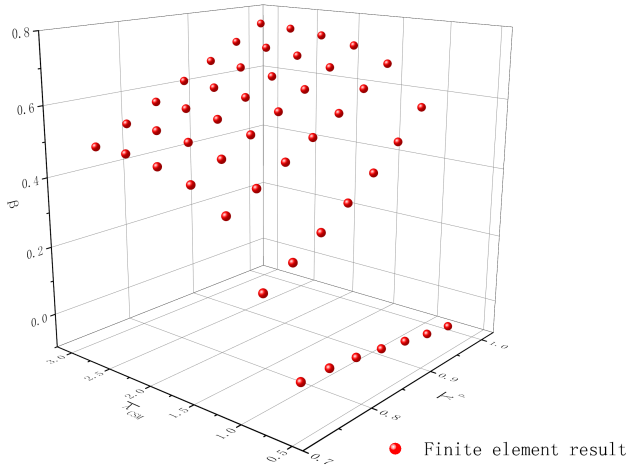

Figure 13. scatter distribution of finite element results when $\bar{\lambda}_p > 0.68$.

When $\bar{\lambda}_p \leq 0.68$, the relationship between β and $\bar{\lambda}_p$, $\bar{\lambda}_{CSM}$ is as follows:

$$\beta = 0.98 - 2.14\bar{\lambda}_{CSM}{}^{-8.64} + 0.02\bar{\lambda}_p^{-1.98} + 0.79\bar{\lambda}_{CSM}{}^{-8.64}\bar{\lambda}_p^{-1.98} \quad (25)$$

The fitting result of Equation (25) is shown in Figure 14. The correlation coefficient R^2 for the fit using Equation (25) is 0.989, indicating a good fitting quality. Additionally, from Equation (25) and Figure 14, it can be seen that as $\bar{\lambda}_p$ approaches 0, β tends to infinity. This result seems to suggest that, from the perspective of the Continuous Strength Method, the strength of the component can grow infinitely as $\bar{\lambda}_p$ approaches 0. However, in practical engineering, the strength of a component obviously cannot increase indefinitely. Furthermore, the load-bearing capacity calculation method for components based on the CSM proposed in this paper is intended to more accurately predict the axial load-bearing capacity of components. Therefore, β cannot tend to infinity and should have an upper limit. In summary, Equation (25) is only applicable for $0.28 \leq \bar{\lambda}_p \leq 0.68$. For the case where $0 < \bar{\lambda}_p < 0.28$, further research is needed to determine the upper limit of β.

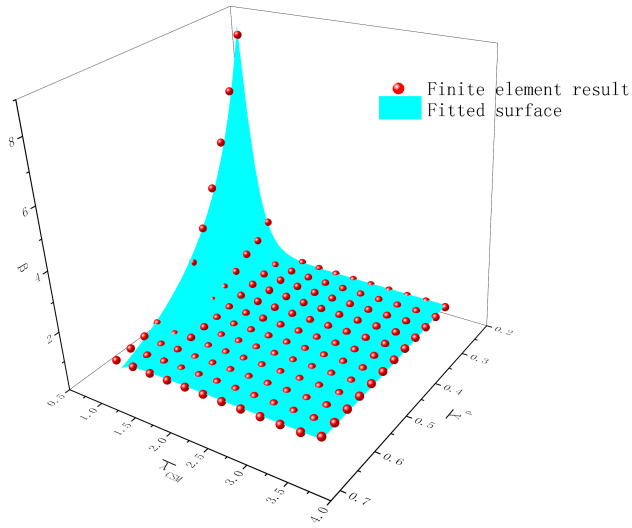

Figure 14. schematic of fitting results when $\bar{\lambda}_p \leq 0.68$.

When $\bar{\lambda}_p > 0.68$, the relationship between β and $\bar{\lambda}_p$, $\bar{\lambda}_{CSM}$ is as follows:

$$\beta = -2.75 + 2.96\exp\left[-\exp\left(\frac{\bar{\lambda}_{CSM} - 0.22}{0.37}\right)\right] - 18.59\exp\left[-\exp\left(\frac{-\bar{\lambda}_p + 0.96}{0.39}\right)\right] + 20\exp\left[-\exp\left(\frac{-\bar{\lambda}_{CSM} - 0.22}{0.37}\right) - \exp\left(\frac{-\bar{\lambda}_p + 0.96}{0.39}\right)\right] \quad (26)$$

the fitting result of Equation (26) is shown in Figure 15. The fit using Equation (25) has a correlation coefficient R^2 of 0.989, indicating that the fit is also of good quality.

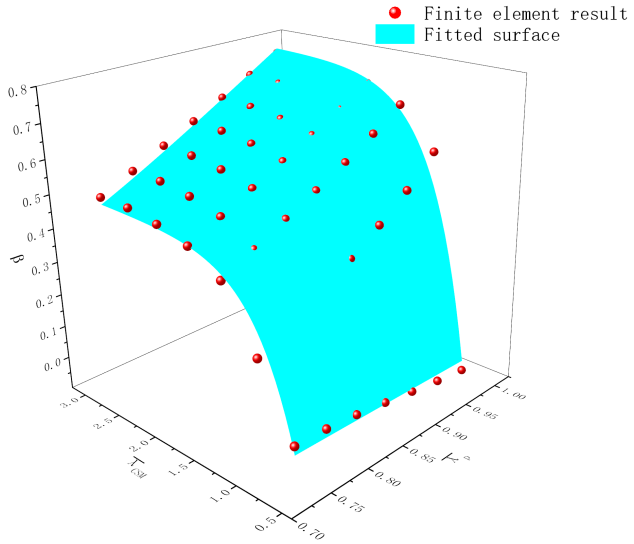

Figure 15. Schematic of fitting results when $\bar{\lambda}_p > 0.68$.

4.5. Computational Workflow

The process for calculating the axial load-bearing capacity of a 7075-T6 aluminum alloy rectangular tube based on the Continuous Strength Method is as follows and Figure 16 is the calculation flowchart

1. Refer to the calculation formula of Continuous Strength Method in reference [13], calculating the section slenderness ratio of structural members $\bar{\lambda}_p$ and the component section strength f_{CSM};
2. Substitute the calculated f_{CSM} into Equation (18) to compute the component's CSM relative slenderness ratio $\bar{\lambda}_{CSM}$;
3. Calculate the component's relative slenderness ratio $\bar{\lambda}$ using Equation (7);
4. Depending on whether $\bar{\lambda}_p \leq 0.68$ or $\bar{\lambda}_p > 0.68$, use either Equation (26) or Equation (27) to compute the strength development index β. It should be noted that Equation (25) also requires $\bar{\lambda}_p \geq 0.28$;
5. Using the results of $\bar{\lambda}_{CSM}$, $\bar{\lambda}$ and β, calculate the CSM stability factor φ_{CSM} using Equations (17), (21), and (23);
6. Substitute φ_{CSM} into the following equation to compute the ultimate bearing capacity result σ_{pre}.

$$\sigma_{pre} = \varphi_{CSM} f_{CSM} \quad (27)$$

The current calculation method is presented based on the analysis of ultimate load-bearing capacity data for 7075-T6 aluminum alloy rectangular tube components with section slenderness ratios $\bar{\lambda}_p$ ranging from 0.28 to 0.99.

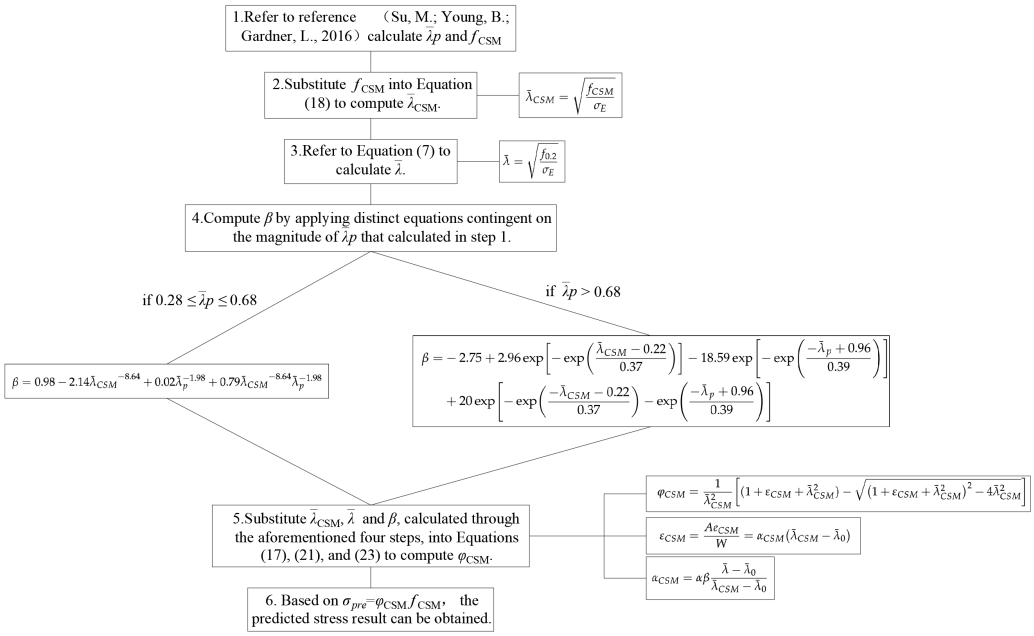

Figure 16. Calculation flowchart [13].

5. Comparison of Calculation Methods

Reference [34] revised the $\varphi-\bar{\lambda}$ curve of Chinese standards based on the axial load-bearing capacity test results of 9 7075-T6 aluminum alloy rectangular tube components. The revised $\varphi-\bar{\lambda}$ curve can be used for the load-bearing capacity calculation of 7075-T6 aluminum alloy rectangular tubes. The axial compression ultimate load-bearing capacities of the nine rectangular tube components were theoretically calculated using both the Continuous Strength Method and the Chinese standard calculation method. The theoretical values based on the Continuous Strength Method are denoted as σ_{prec}, while those based on the revised Chinese standard method are denoted as σ_{prer}. The predictions by Eurocode 9 [6] are denoted as σ_{pree}, and by AA-ADM 2020 [21] as σ_{prea}. The ratio of these theoretical values to the measured load-bearing capacity results is used as an indicator of the deviation. The results are shown in Table 6.

Table 6. Comparison of Experimental Results with Computational Results from Two Methods.

Number of the Specimen	σ_t /MPa	σ_{prec} /MPa	σ_{prec}/σ_t	σ_{prer} /MPa	σ_{prer}/σ_t	σ_{pree} /MPa	σ_{pree}/σ_t	σ_{prea} /MPa	σ_{prea}/σ_t
40-40-5-30	388.1	282.71	0.73	372.2	0.96	239.75	0.62	252.45	0.65
40-40-5-45	319.6	253.60	0.79	267.11	0.84	194.29	0.61	192.87	0.60
40-40-5-60	192.3	169.77	0.88	169.89	0.88	135.06	0.70	117.45	0.61
60-40-3-30	442.6	349.08	0.79	195.30	0.44	286.02	0.65	227.06	0.51
60-40-3-45	262.2	303.00	1.16	156.61	0.6	311.56	1.19	168.23	0.64
60-40-3-60	192.9	183.32	0.95	96.99	0.5	194.20	1.01	94.63	0.49
80-60-3-30	297.9	284.65	0.96	246.18	0.83	326.89	1.10	384.05	1.29
80-60-3-45	230.1	266.98	1.16	182.79	0.79	202.36	0.88	220.52	0.96
80-60-3-60	172.5	180.67	1.05	114.58	0.66	135.26	0.78	134.90	0.78
Average	——	——	0.94	——	0.72	——	0.84	——	0.73
Variance	——	——	0.02	——	0.03	——	0.04	——	0.06

From Table 6, it can be seen that the average value of σ_{prec}/σ_t is higher than that of others and is closer to 1. The differences in variance among the four results are very small, indicating that the degree of deviation and dispersion are similar for the four methods.

However, the results based on the Continuous Strength Method are closer to the actual measured values. Therefore, the calculation method proposed in this paper based on the Continuous Strength Method is considered to be reasonably valid.

However, for components 60-40-3-45, 80-60-3-45, and 80-60-3-60, this method overestimates the load-bearing capacity. The reason is that the cross-sections of these components belong to type four of sections defined in Eurocode 9 [6], where the strength is controlled by local buckling of the plates. The Continuous Strength Method may overestimate the strength of these sections, leading to an overestimated load-bearing capacity. After excluding these three specimens, the average values of σ_{prec}/σ_t , σ_{prer}/σ_t , σ_{pree}/σ_t and σ_{prea}/σ_t are 0.85, 0.74, 0.84, and 0.73, respectively, with variances of 0.0089, 0.047, 0.039, and 0.075. It can be seen that the results based on the Continuous Strength Method are closer to the experimental results, with smaller dispersion.

6. Conclusions

Based on the axial load-bearing capacity test results of 9 7075-T6 aluminum alloy rectangular tube components and the calculation results of 215 finite element models, and using the basic curves and constitutive model provided by Su, this paper proposes a method for calculating the stability factor of aluminum alloy rectangular tube components based on the Continuous Strength Method (CSM). The specific conclusions are as follows:

(1) In the component load-bearing capacity calculation method based on the Continuous Strength Method, the parameter β can be calculated using Equations (25) or (26) based on the section slenderness ratio $\bar{\lambda}_p$ and the CSM relative slenderness ratio $\bar{\lambda}_{CSM}$. However, this requires $\bar{\lambda}_p \geq 0.28$. For cases where $0 < \bar{\lambda}_p < 0.28$; further research is needed to determine the upper limit of β.

(2) The component load-bearing capacity calculation method based on the Continuous Strength Method proposed in this paper can more accurately predict the axial load-bearing capacity of 7075-T6 aluminum alloy rectangular tube components compared with the modified Chinese standard method and the calculation methods in Eurocode 9 [6] and AA ADM-2020 [21]. This provides a reference for the further promotion and application of the Continuous Strength Method. However, for components with section types falling under the fourth category of sections, the proposed method may overestimate the load-bearing capacity, further investigation is warranted to comprehensively address this issue.

Author Contributions: Z.H.: Conceptualization, Methodology, Funding acquisition and Writing—review and editing. H.L.: Software, Validation, Investigation, and Writing—original draft. C.Z.: Project administration. J.L.: Formal analysis; Supervision and Resources. All authors have read and agreed to the published version of the manuscript.

Funding: This research was supported by the Research on Highway Supervision Management System Based on the Integration of Oblique Photography and BIM Technology (QD2022-174-087), Guangxi Key Laboratory of Green Building Materials and Construction Industrialization, and Guangxi Science and Technology Program (Project No. AD25069101).

Data Availability Statement: Further inquiries can be directed to the corresponding authors.

Acknowledgments: The authors would like to express their sincere gratitude to Liu Junli for his invaluable guidance and meticulous revisions of the manuscript, which greatly improved the quality of this work. We appreciate the constructive discussions and technical contributions from all team members, which enriched the research outcomes. Finally, we acknowledge the facilities and resources provided by our institution, which enabled this research. We thank ABAQUS/CAE [https://www.3ds.com/products/simulia/abaqus/cae, accessed on 7 April 2025] for its assistance during the simulation and analysis process.

Conflicts of Interest: The authors declare that they do not have any competing financial interests or personal relationships that could have appeared to influence the work presented in this paper.

References

1. Shen, Z.; Guo, X.; Li, Y. A Brief Review of the Research Status of Aluminum Alloy Structures. *J. Build. Struct.* **2007**, *28*, 100–109.
2. Raabe, D.; Ponge, D.; Uggowitzer, P.J.; Roscher, M.; Paolantonio, M.; Liu, C.; Antrekowitsch, H.; Kozeschnik, E.; Seidmann, D.; Gault, B.; et al. Making sustainable aluminum by recycling scrap: The science of 'dirty' alloys. *Prog. Mater. Sci.* **2022**, *128*, 100947. [CrossRef]
3. You, X.; Xing, Z.; Jiang, S.; Zhu, Y.; Lin, Y.; Qiu, H.; Nie, R.; Yang, J.; Hui, D.; Chen, W.; et al. A Review of Research on Aluminum Alloy Materials in Structural Engineering. *Dev. Built Environ.* **2024**, *17*, 100319. [CrossRef]
4. *GB/T 50429-2007*; Code for Design of Aluminum Alloy Structures. China Planning Press: Beijing, China, 2007.
5. Zhang, Q.; Ji, J.; Yang, L.; Wu, M. Several Important Concepts and Research Bases in the 'Code for Design of Aluminum Alloy Structures. *J. Build. Struct.* **2009**, *30*, 1–12.
6. *EN 1999-1-1:2007+A1*; Eurocode 9: Design of Aluminium Structures–Part 1-1: General Structural Rules. European Committee for Standardization (CEN): Brussels, Belgium, 2009.
7. Wang, Y.; Chang, T.; Shi, Y.; Yuan, H.; Yin, J.; Ouyang, Y. Experimental Study on Local Buckling of Short Columns with Aluminum Alloy Open Sections Under Axial Compression. *J. Build. Struct.* **2015**, *36*, 46–53.
8. Chen, X.; Fan, J.; Guo, R. Influence of Plate Group Effects on the Sectional Bearing Capacity of Rectangular Thin-Walled Members. *J. Kunming Univ. Sci. Technol. (Nat. Sci. Ed.)* **2009**, *34*, 57–61.
9. Kang, Y.; Yang, Y.; Huang, J.; Zhu, J. An experimental study on dynamic constitutive relationship of 7075-T651 aluminum alloy. *Adv. Mater. Res.* **2013**, *816*, 84–89. [CrossRef]
10. Gardner, L. The continuous strength method. *Proc. Inst. Civ. Eng.–Struct. Build.* **2008**, *161*,127–133. [CrossRef]
11. Gardner, L.; Yun, X.; Walport, F. The continuous strength method—Review and outlook. *Eng. Struct.* **2023**, *275*, 114924. [CrossRef]
12. Su, M.; Young, B.; Gardner, L. Flexural response of aluminum alloy SHS and RHS with internal stiffeners. *Eng. Struct.* **2016**, *121*, 170–180. [CrossRef]
13. Su, M.; Young, B.; Gardner, L. The continuous strength method for the design of aluminum alloy structural elements. *Eng. Struct.* **2016**, *122*, 338–348. [CrossRef]
14. Su, M.; Young, B.; Gardner, L. Deformation-based design of aluminum alloy beams. *Eng. Struct.* **2014**, *80*, 339–349. [CrossRef]
15. Su, M.; Young, B.; Gardner, L. Testing and Design of Aluminum Alloy Cross Sections in Compression. *J. Struct. Eng.* **2014**, *140*, 04014047. [CrossRef]
16. Su, M.; Young, B.; Gardner, L. Continuous strength method for aluminium alloy structures. *Adv. Mater. Res.* **2013**, *742*, 70–75. [CrossRef]
17. Bock, M.; Theofanous, M.; Dirar, S.; Lipitkas, N. Aluminum SHS and RHS subjected to biaxial bending: Experimental testing, modelling and design recommendations. *Eng. Struct.* **2021**, *227*, 111468. [CrossRef]
18. Buchanan, C.; Gardner, L.; Liew, A. The continuous strength method for the design of circular hollow sections. *J. Constr. Steel Res.* **2016**, *118*, 207–216. [CrossRef]
19. Chen, X.; Li, W.; Lu, X.; Lian, M. Study on the Stability and Bearing Capacity of Aluminum Alloy Box-Section Axial Compression Members Based on the Continuous Strength Method. *J. Shenyang Jian Zhu Univ. (Nat. Sci. Ed.)* **2022**, *38*, 401–409.
20. *Aluminum Design Manual: Specification & Guidelines for Aluminum Structures*; The Aluminum Association: Arlington, VA, USA, 2015.
21. *Aluminum Design Manual: Specification & Guidelines for Aluminum Structures*; The Aluminum Association: Arlington, VA, USA, 2020.
22. Zhai, X.; Sun, L.; Zhao, Y. Comparison of Stability Bearing Capacity of High-Strength Aluminum Alloy Compression-Bending Members between Chinese and European Codes. *J. Harbin Inst. Technol.* **2015**, *47*, 1–8.
23. Zhai, X.; Qi, R.; Zhao, Y. Calculation Methods for Flexural Bearing Capacity of 6082-T6 Aluminum Alloy Members. *J. Harbin Inst. Technol.* **2018**, *50*, 192–198.
24. Zhai, X.; Sun, L.; Zhao, Y. Study on Stability Bearing Capacity of 6082-T6 Aluminum Alloy Box and L-Shaped Section Compression-Bending Members. *J. Build. Struct.* **2015**, *36*, 73–82.
25. Zhao, Y.; Zhai, X.; Sun, L. Test and design method for the buckling behaviors of 6082-T6 aluminum alloy columns with box-type and L-type sections under eccentric compression. *Thin-Walled Struct.* **2016**, *100*, 62–80. [CrossRef]
26. Zhao, Y.; Zhai, X. Reliability assessment of aluminum alloy columns subjected to axial and eccentric loadings. *Struct. Saf.* **2018**, *70*, 1–13. [CrossRef]
27. Chen, L.; Xu, W.; Chen, Y.; Sun, W. A new continuous strength method for prediction of strain-hardening performance of high-strength aluminum alloy cylindrical columns. *Buildings* **2024**, *14*, 3055. [CrossRef]

28. *GB/T 228.1 or ISO 6892-1*; Metallic Materials—Tensile Testing—Part 1: Method of Test at Room Temperature. China Iron and Steel Association: Beijing, China, 2021.
29. Ramberg, W.; Osgood, W.R. *Description of Stress-Strain Curves by Three Parameters*; NACA TN-902: Washington, DC, USA, 1943.
30. SteinHardt, O. Aluminum constructions in civil engineering. *Aluminum* **1971**, *47*, 131–139.
31. Guo, X. Theoretical and Experimental Research on Aluminum Alloy Structural Members. Ph.D. Dissertation, Tongji University, Shanghai, China, 2006.
32. Seif, M.; Schafer, W.B. Local buckling of structural steel shapes. *J. Constr. Steel Res.* **2010**, *66*, 1232–1247. [CrossRef]
33. Paczos, P.; Pawlak, A.M. Experimental Optical Testing and Numerical Verification by CUFSM of Compression Columns with Modified Channel Section. *Materials* **2021**, *14*, 1271. [CrossRef]
34. Li, H. Experimental Study on the Axial Compression Performance and Bearing Capacity Calculation Method of 7075-T6 Aluminum Alloy Rectangle Tubes. Master's Thesis, Guilin University of Technology, Guilin, China, 2024.